Supporting Information

$Ni_{12}P_5$ Nanoparticles Binding on Graphene Sheets toward Advanced Lithium−Sulfur Batteries

Guangzeng Liu,*[,†,‡] Zhengchunyu Zhang,[‡] Wenzhi Tian,[‡] Weihua Chen,[&] Baojuan Xi,[‡] Haibo Li,[¶] Jinkui Feng,[#] and Shenglin Xiong[‡]

[†] School of Chemistry and Chemistry Engineering, Qilu Normal University, Jinan, 250200, P. R. China.

[‡] Key Laboratory of Colloid and Interface Chemistry, Ministry of Education, School of Chemistry and Chemical Engineering, and State Key Laboratory of Crystal Materials, Shandong University, Jinan, 250100, P. R. China

[&] Key Laboratory of Material Processing and Mold of Ministry of Education, Zhengzhou University, Zhengzhou 450001, P. R. China

[¶] School of Chemistry and Chemical Engineering, Liaocheng University, Liaocheng, Shandong 252059, P. R. China

[#] Key Laboratory for Liquid-Solid Structural Evolution and Processing of Materials, Ministry of Education, School of Materials Science and Engineering, Shandong University, Jinan 250061, P. R. China

*E-mail: gzliusd@163.com

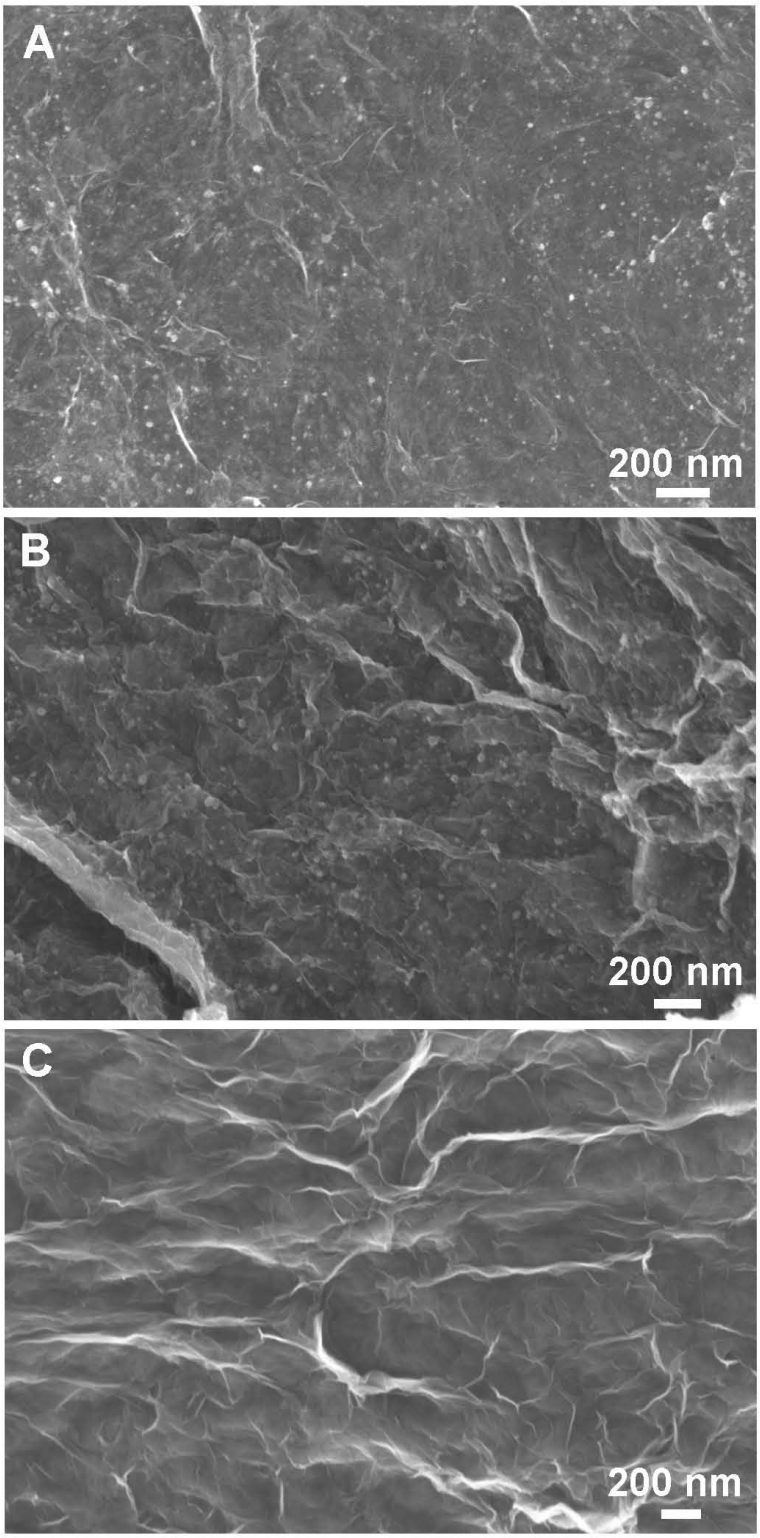

Figure S1. FESEM images of the precursor I (A), precursor II (B) and (C) precursor III.

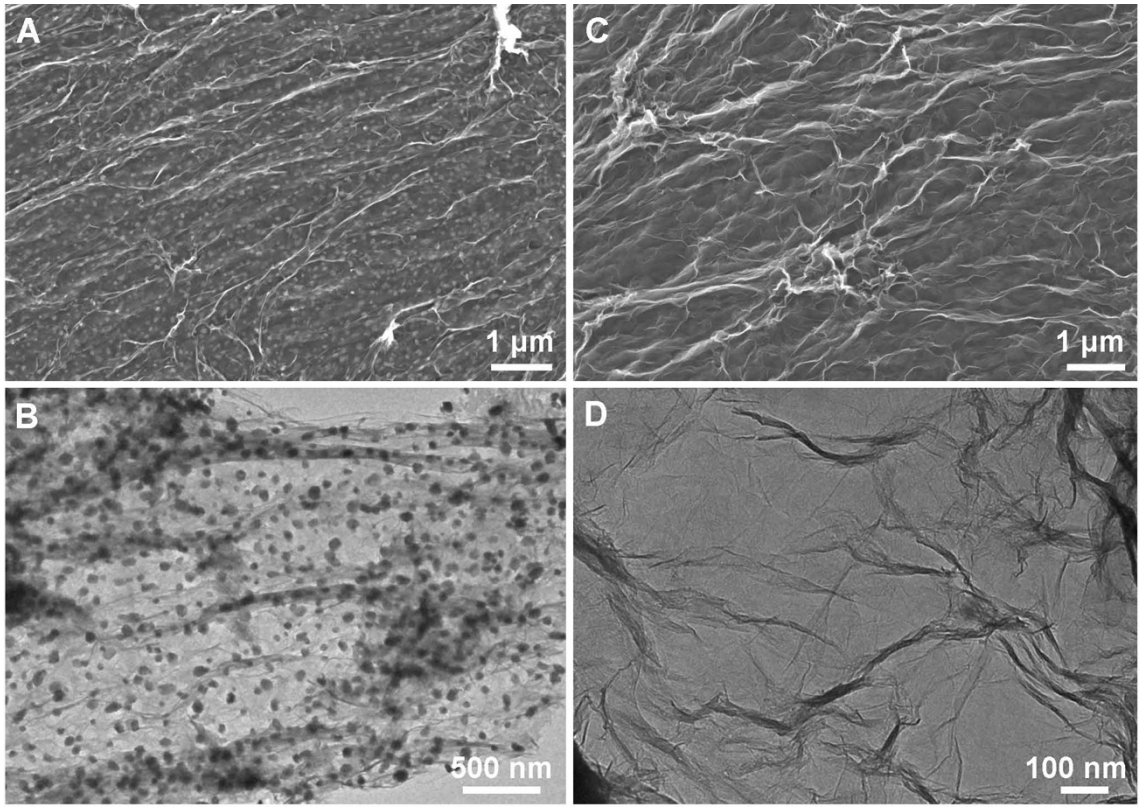

Figure S2. FESEM and TEM images of (A,C) Ni_9S_8@ rGO and (B,D) rGO.

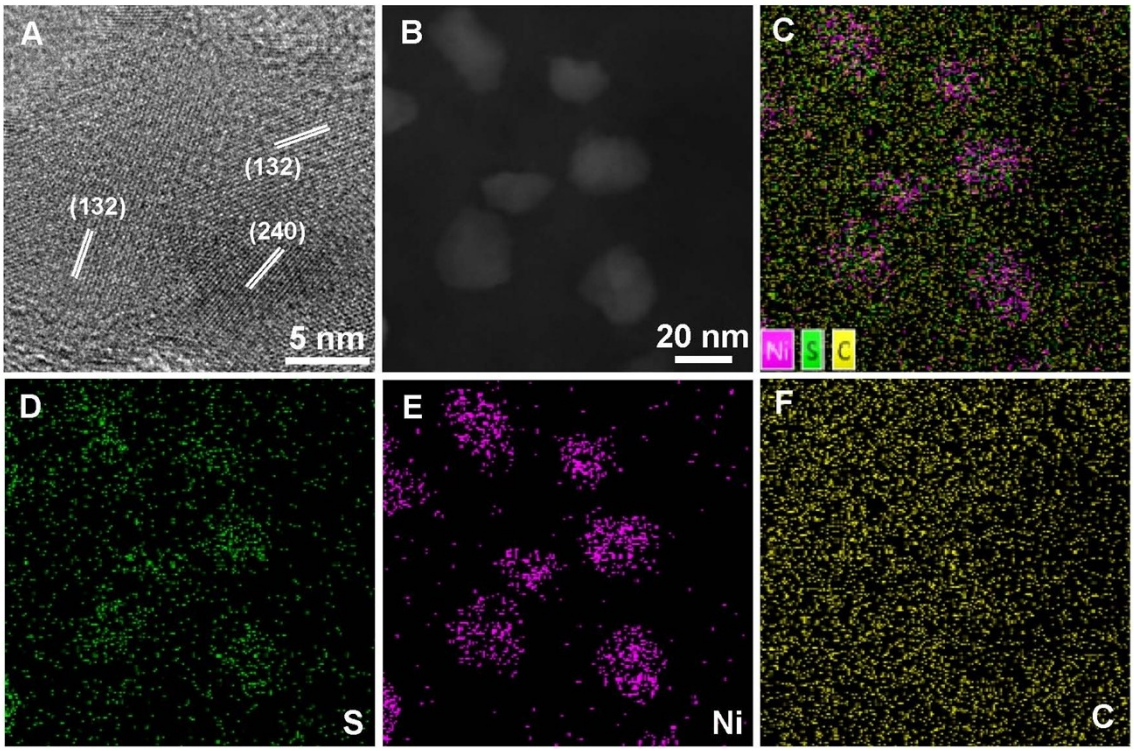

Figure S3. (A) HRTEM image of Ni_9S_8@rGO, (B) TEM image of Ni_9S_8@rGO nanosheets, and the corresponding mappings of (C) merged image, (D) S, (E) Ni, and (F) C.

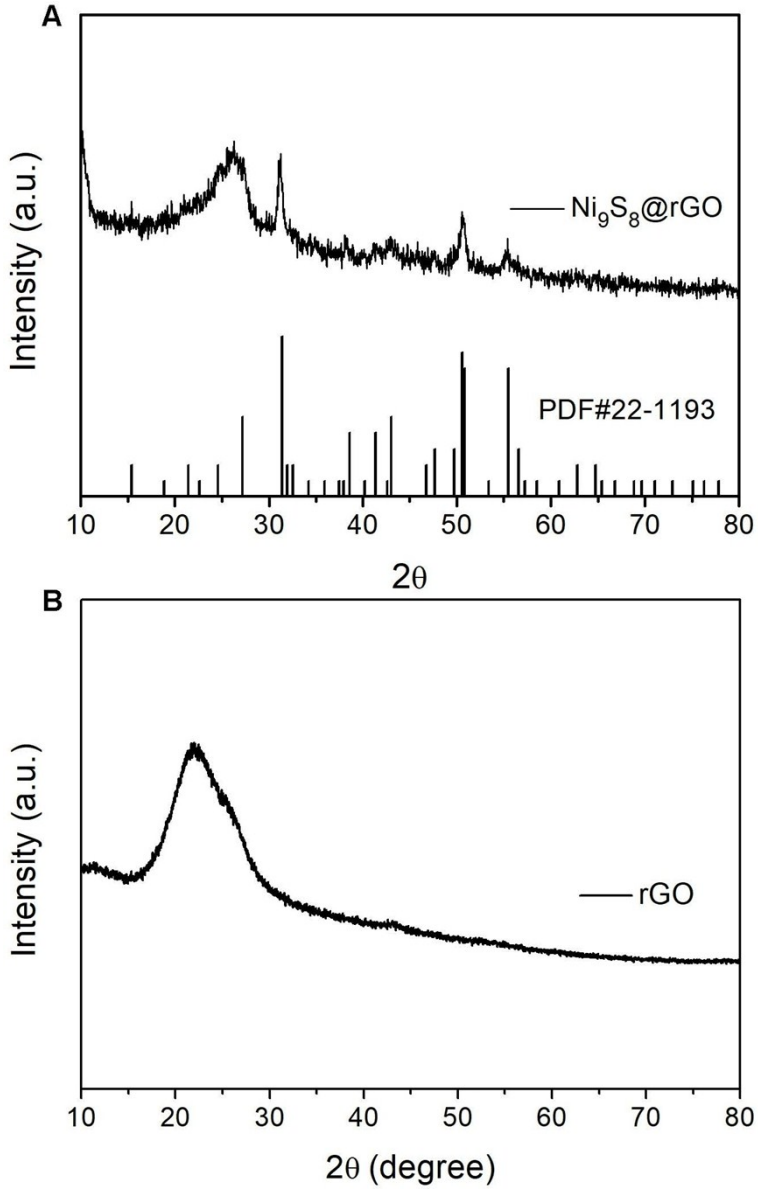

Figure S4. The XRD patterns of Ni_9S_8@rGO nanosheets (A) and rGO (B).

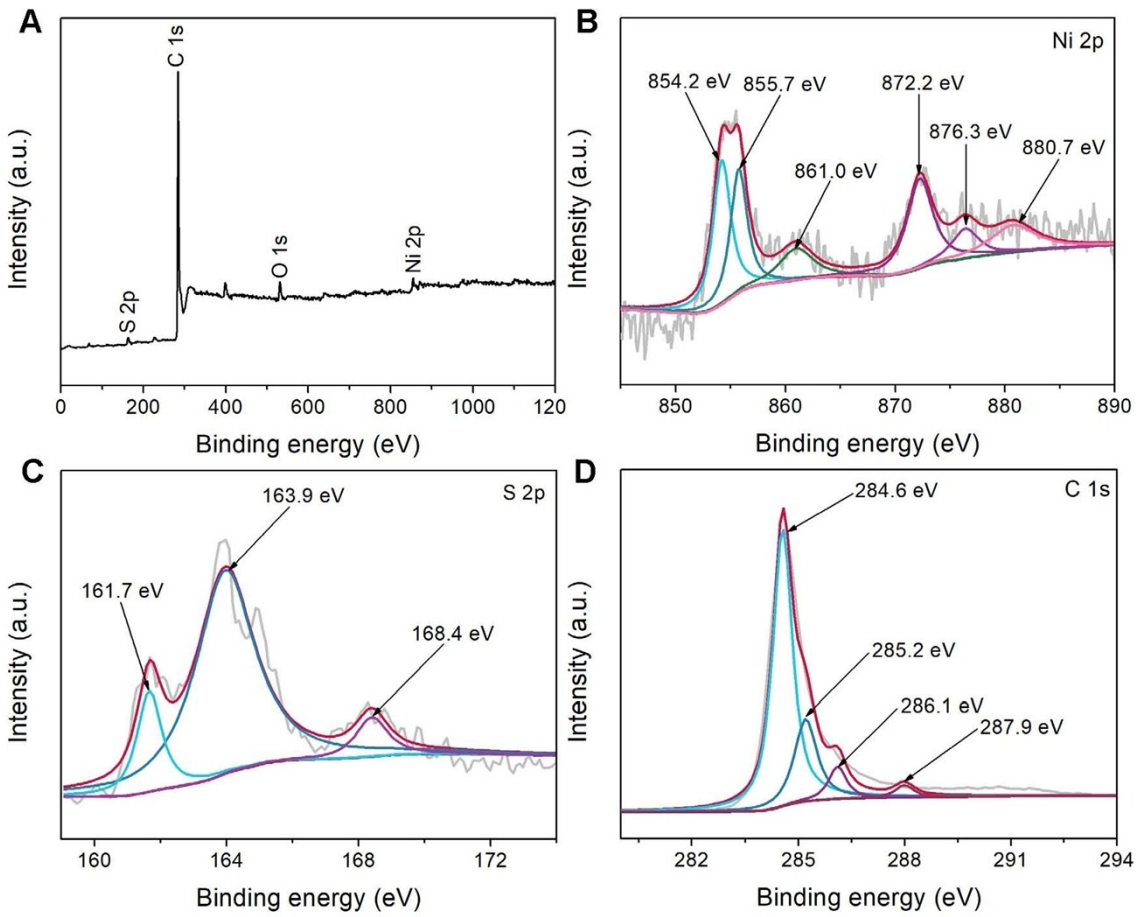

Figure S5. XPS spectra of Ni_9S_8@rGO nanosheets: (A) survey, (B-D) high-resolution spectra of Ni 2p, S 2p, and C 1s.

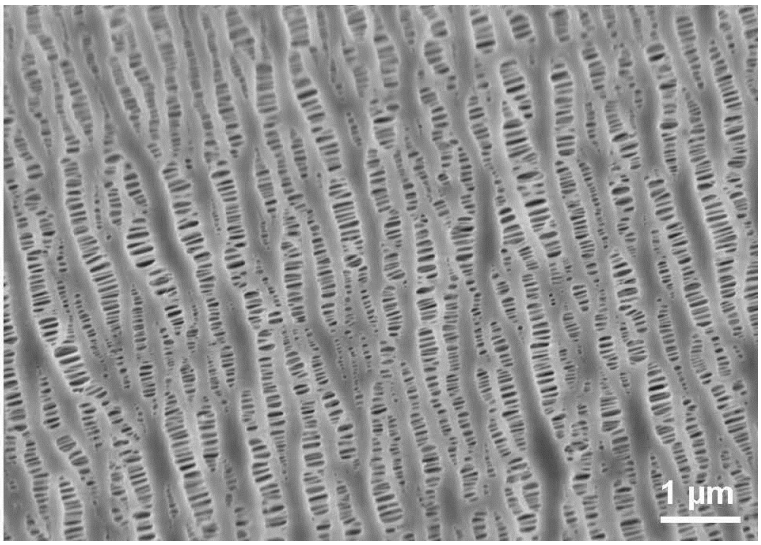

Figure S6. The pristine 2400 Celgard film.

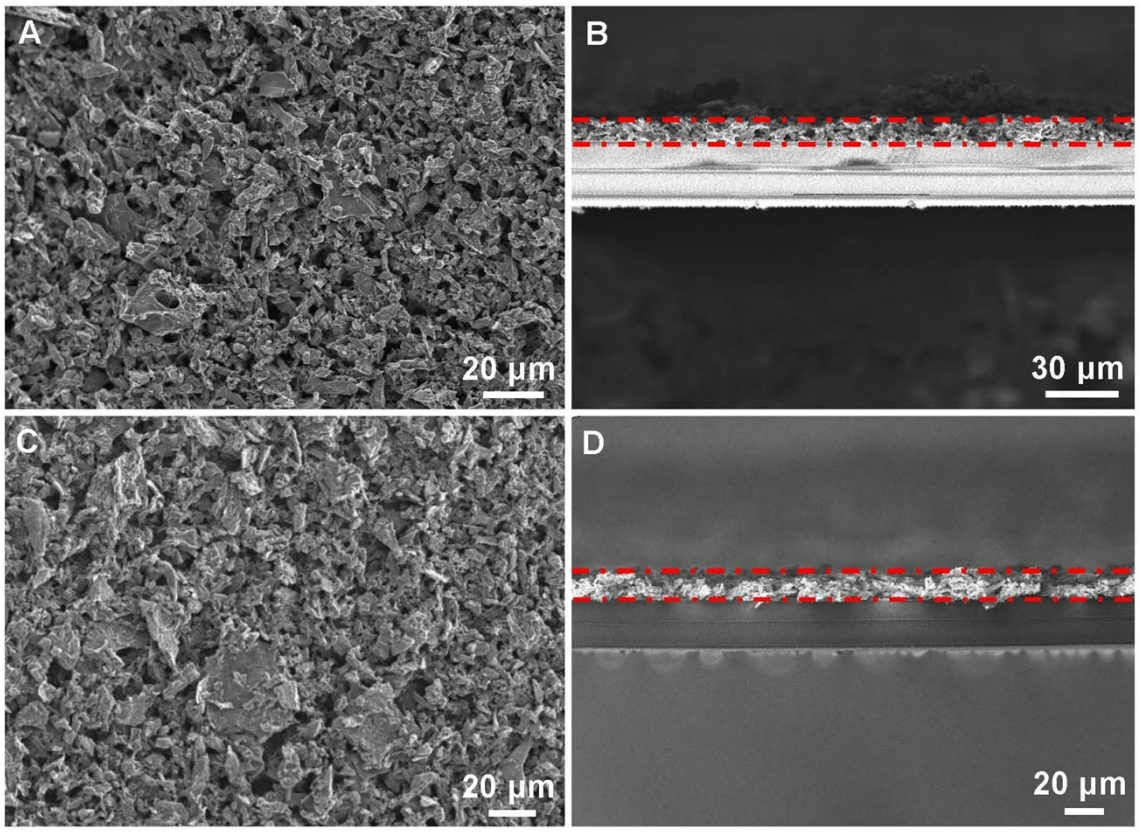

Figure S7. FESEM images of top surface and cross-section of (A, B) Ni_9S_8@rGO, (C, D) rGO.

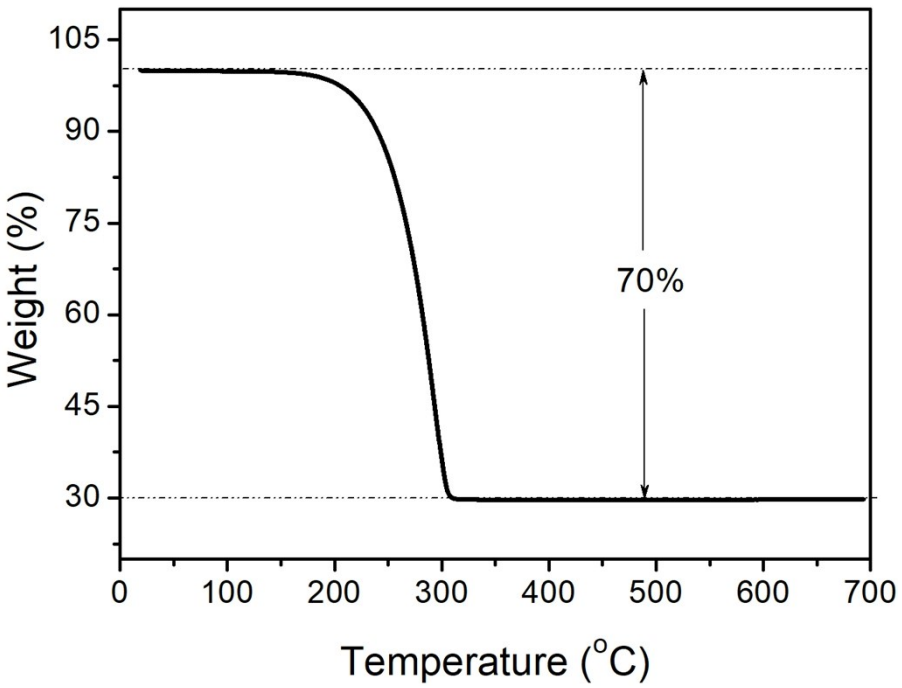

Figure S8. The TGA curve of the composite of sulfur and acetylene black in nitrogen atmosphere.

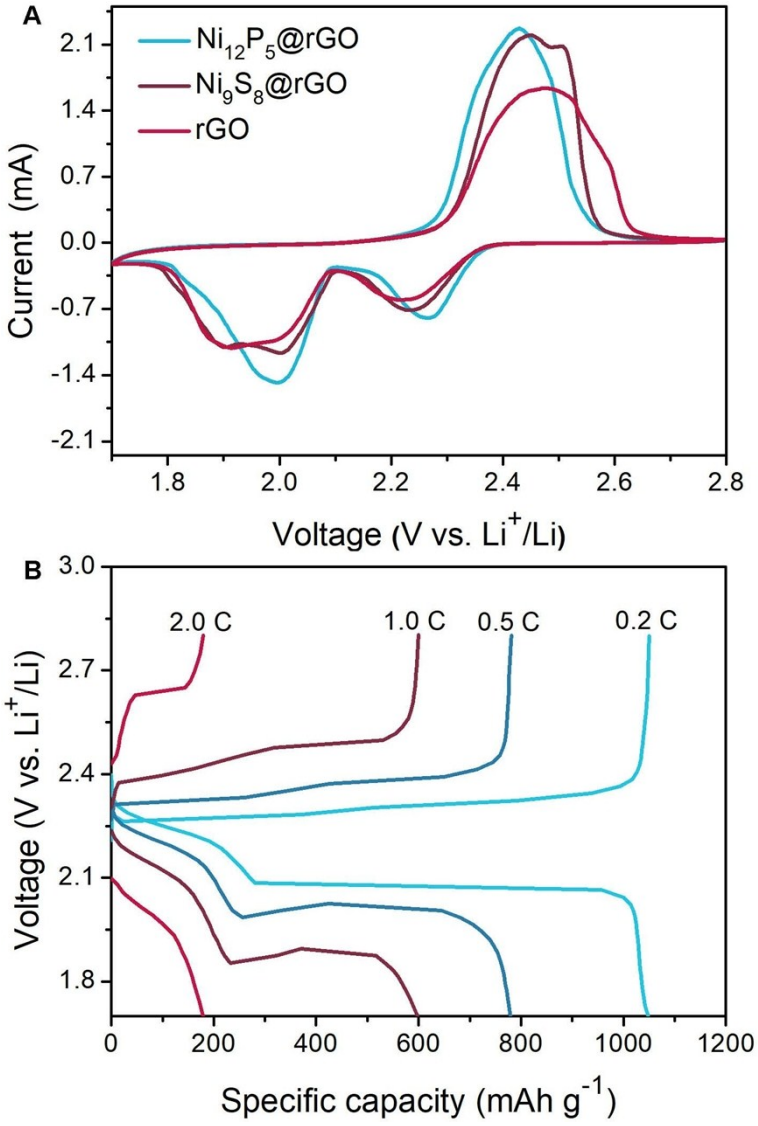

Figure S9. (A) The CV curves for the third cycle of cells with $Ni_{12}P_5$@rGO, Ni_9S_8@rGO and rGO separators at the scan rate of 0.1 mV s^{-1}, (B) the galvanostatic charge/discharge voltage curves at different current densities of the cell with the pristine separator.

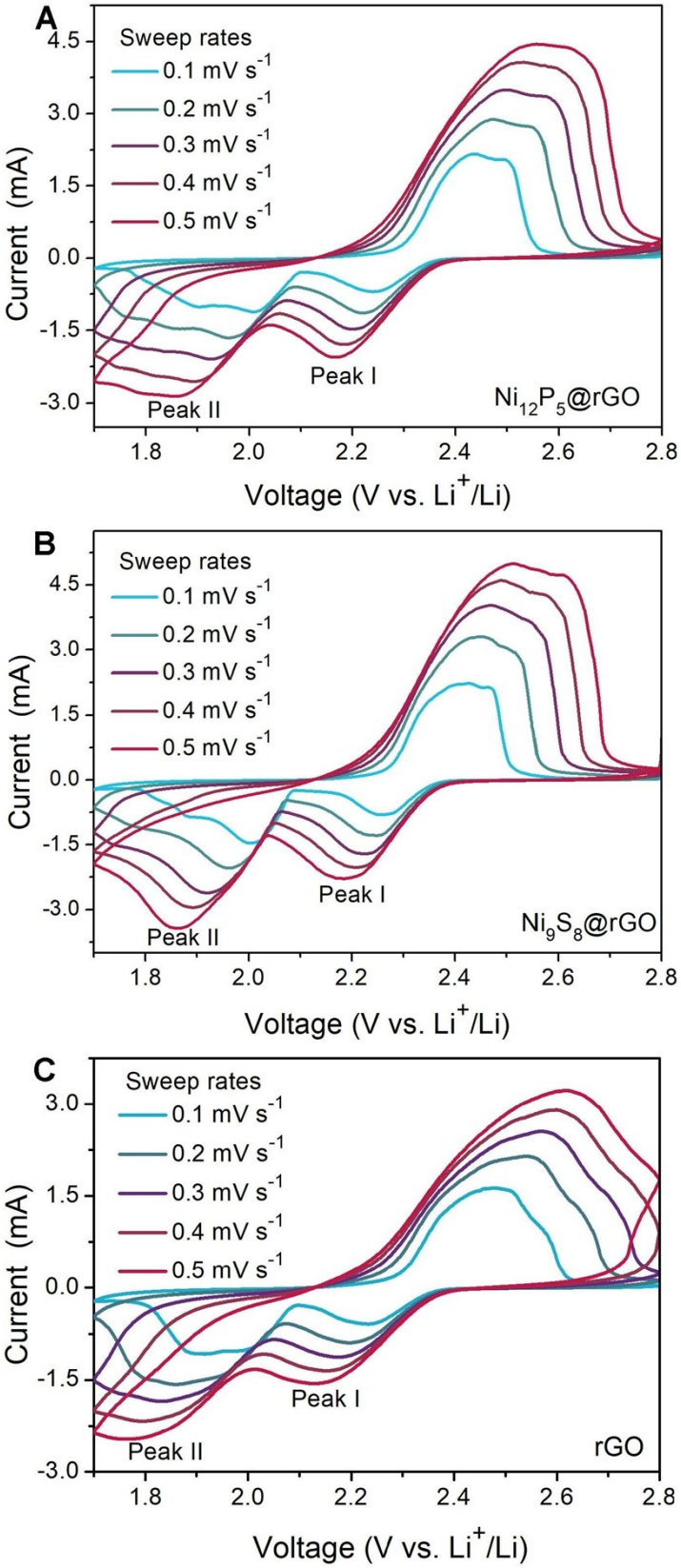

Figure S10. The CV curves at different sweep rates of (A) S//$Ni_{12}P_5$@rGO, (B)

S//Ni_9S_8@rGO and (C) S//rGO.

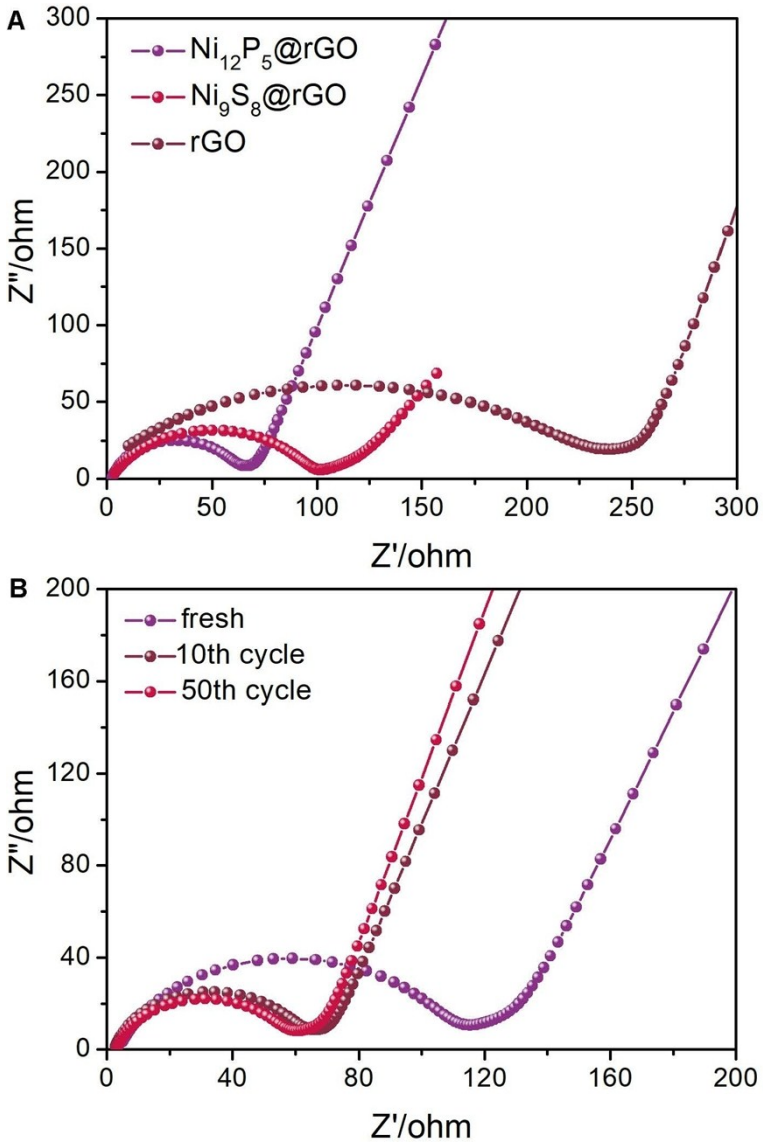

Figure S11. (A) The electrochemical impedance spectra (EIS) of S//$Ni_{12}P_5$@rGO, S//Ni_9S_8@rGO and S//rGO cells after 10 cycles at 0.5 C. (B) The EIS of the S//$Ni_{12}P_5$@rGO cell after different discharge/charge cycles at 0.5 C.

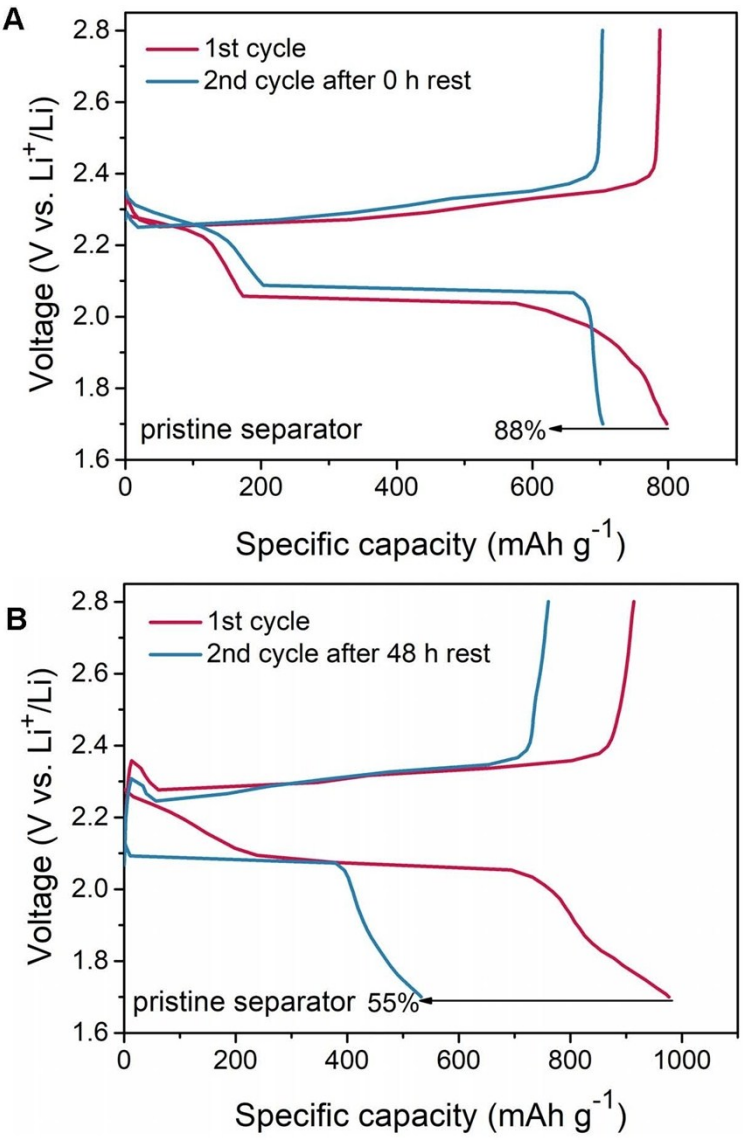

Figure S12. The discharge/charge curves of S//pristine separator cell at 0.2 C: (A) rest for 0 h, (B) rest for 48 h.

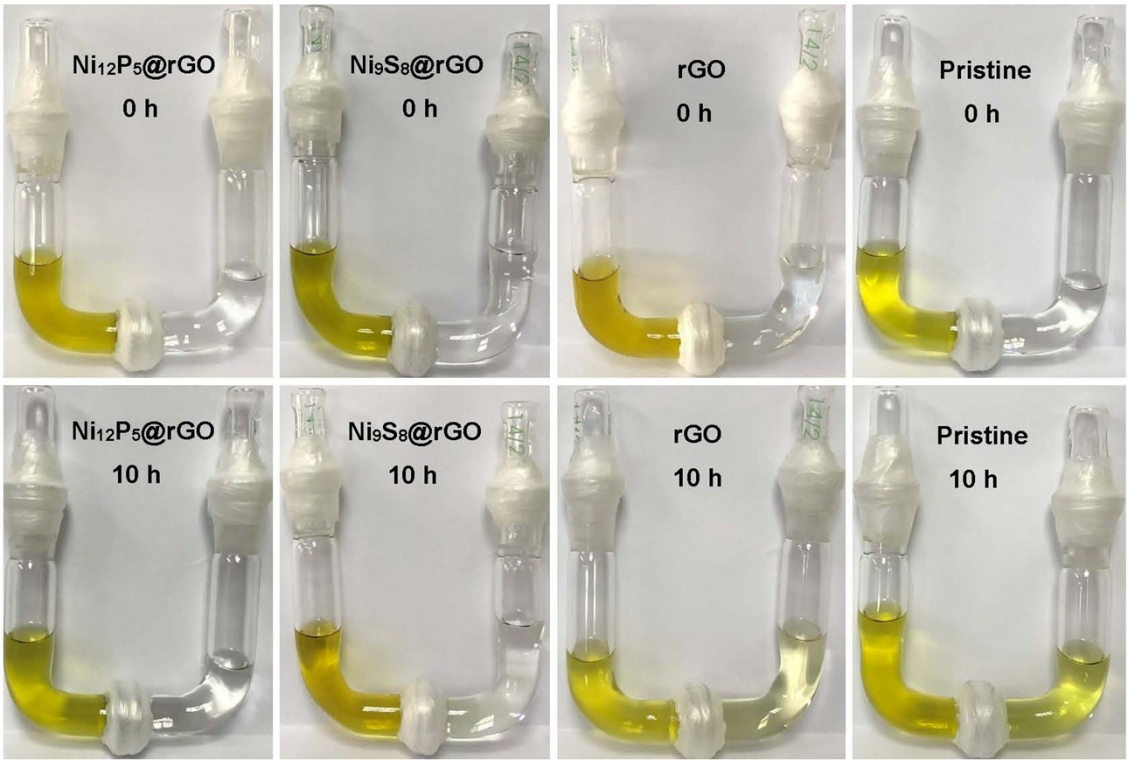

Figure S13. The Li_2S_6 permeability experiments of different functional separators.